BIOCHEMISTRY
including biophysical chemistry & molecular biology

Article

pubs.acs.org/biochemistry

Conservation of Dark Recovery Kinetic Parameters and Structural Features in the Pseudomonadaceae "Short" Light, Oxygen, Voltage (LOV) Protein Family: Implications for the Design of LOV-Based Optogenetic Tools

Raj Rani,[†] Katrin Jentzsch,[†] Justin Lecher,[‡] Rudolf Hartmann,[‡] Dieter Willbold,[‡,§] Karl-Erich Jaeger,[†] and Ulrich Krauss*[,†]

[†]Institut für Molekulare Enzymtechnologie, Heinrich-Heine-Universität Düsseldorf, Forschungszentrum Jülich, Stetternicher Forst, D-52426 Jülich, Germany

[‡]Institute of Complex Systems, ICS-6, Forschungszentrum Jülich, Jülich, Germany

[§]Institut für Physikalische Biologie, Heinrich-Heine-Universität Düsseldorf, Düsseldorf, Germany

Supporting Information

ABSTRACT: In bacteria and fungi, various light, oxygen, voltage (LOV) sensory systems that lack a fused effector domain but instead contain only short N- and C-terminal extensions flanking the LOV core exist. In the prokaryotic kingdom, this so-called "short" LOV protein family represents the third largest LOV photoreceptor family. This observation prompted us to study their distribution and phylogeny as well as their photochemical and structural properties in more detail. We recently described the slow and fast reverting "short" LOV proteins PpSB1-LOV and PpSB2-LOV from *Pseudomonas putida* KT2440 whose adduct state lifetimes varied by 3 orders of magnitude [Jentzsch, K., Wirtz, A., Circolone, F., Drepper, T., Losi, A., Gärtner, W., Jaeger, K. E., and Krauss, U. (2009) *Biochemistry 48*, 10321−10333]. We now present evidence of the conservation of similar fast and slow-reverting "short" LOV proteins in different *Pseudomonas* species. Truncation studies conducted with PpSB1-LOV and PpSB2-LOV suggested that the short N- and C-terminal extensions outside of the LOV core domain are essential for the structural integrity and folding of the two proteins. While circular dichroism and solution nuclear magnetic resonance experiments verify that the two short C-terminal extensions of PpSB1-LOV and PpSB2-LOV form independently folding helical structures in solution, bioinformatic analyses imply the formation of coiled coils of the respective structural elements in the context of the dimeric full-length proteins. Given their prototypic architecture, conserved in most more complex LOV photoreceptor systems, "short" LOV proteins could represent ideally suited building blocks for the design of genetically encoded photoswitches (i.e., LOV-based optogenetic tools).

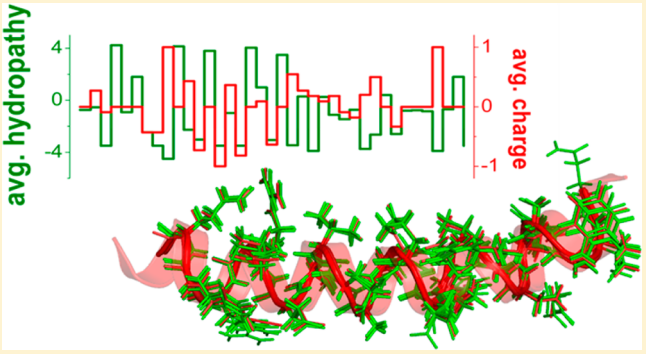

Light, oxygen, voltage (LOV) photoreceptors are ubiquitously distributed, functionally versatile, multidomain sensory systems,[1,2] whose blue light-sensitive LOV domains show a conserved Per-Arnt-Sim (PAS) fold.[3] Like other PAS domains,[3] LOV domains bind a small molecule ligand [i.e., flavin mononucleotide (FMN)] that mediates initial signal perception.[4] Hereby, LOV domains undergo a blue light-dependent photocycle, which intricately links flavin photochemistry and protein structural rearrangements in the vicinity of the FMN molecule to larger scale conformational changes of N- and C-terminally located structural elements outside of the conserved sensor core domain.[4] In multidomain LOV photoreceptors, those latter structural elements link the sensor domain with a variety of different effector domain modules such as kinases, phosphodiesterases, DNA-binding domains, and transcription factors.[1,5,6] In most recent studies, those auxiliary elements are termed the N-terminal cap (N-cap) and C-terminal Jα-helix.[7−11] For many of the previously studied LOV photoreceptor proteins, removal of those elements is possible without impairing folding and photocycling. In fact, most LOV domain X-ray structures were initially obtained for truncated constructs consisting only of the conserved sensor core domain.[12−14] More recently, it became evident that, for example, the interaction of those linker elements with the sensor core domain can be modulated by blue light, eventually facilitating the biological response.[4,6] In the rapidly growing field of LOV-based optogenetics, this relay mechanism is exploited to confer light-dependent control to non-photo-

Received: March 11, 2013
Revised: May 27, 2013
Published: June 7, 2013

dx.doi.org/10.1021/bi400311r | *Biochemistry* 2013, 52, 4460−4473

sensitive enzymes and proteins.[15−21] In conclusion, the orientation and structure of the N- and C-terminal elements outside the conserved sensor core is of primary importance for understanding LOV- and PAS-based signaling responses[4,6,7] and can provide a rational basis for the design of LOV-based optogenetic switches.[16] While those N- and C-terminal elements apparently make up a conserved part of most LOV photoreceptors,[4,6,7] their sequence as well as the mode and degree of interaction between them and the sensory core domain varies from system to system.[4,18]

In bacteria and fungi, a subset of LOV photoreceptors that lack fused effector domains exist. Those proteins either possess only an N-cap (*Neurospora crassa* VVD[22]) or contain both N-cap and Jα structural elements (*Pseudomonas putida* PpSB1-LOV and PpSB2-LOV[7] and RsLOV of *Rhodobacter sphaeroides* 2.4.1[23,24]). In bacteria, "short" LOV proteins are present in approximately 11−13% of fully sequenced bacterial genomes.[5] This renders them the third largest LOV protein family in the prokaryotic kingdom.[5] Although "short" LOV proteins lack associated effector domains, a physiological function has been attributed to *N. crassa* VVD and recently also to RsLOV.[23,24] While VVD modulates gating of the circadian clock via interaction with the White-Collar Complex (WCC), the central transcription factor of the circadian clock in *N. crassa*,[22] RsLOV, was suggested to act as a repressor of photosynthesis gene expression and was linked to photooxidative damage responses, carbohydrate metabolism, and chemotaxis.[24]

We recently described a set of two "short" LOV proteins, PpSB1-LOV and PpSB2-LOV, from the saprotrophic microbe *P. putida* KT2440.[25,26] The two proteins are highly similar with respect to their amino acid sequence (approximately 66% identical amino acids) but display drastically different photocycle kinetic properties.[25,26] The light state X-ray structure determined for the slow-cycling PpSB1-LOV protein revealed a canonical LOV core domain with short helical N- and C-terminal extensions (N-cap and Jα-helix, respectively).[7] Both of the latter structural elements facilitate assembly of the parallel homodimer in the crystal. Hereby, the C-terminal Jα-helices, which protrude from the subunit core, contribute to dimer stability by supporting subunit assembly via a coiled-coil-like interaction promoted by hydrophobic residues buried in the Jα dimer interface.[7] Thus, it is of considerable interest whether variable dark recovery kinetic properties as well as the respective auxiliary structural features are conserved among the family of "short" LOV proteins. Although the recent X-ray structure provides the first insights into the structural role of both N- and C-terminal extensions, their role for folding of the full-length "short" LOV proteins in solution is yet ill defined.

To address evolutionary conservation of "short" LOV proteins, we here study the distribution and phylogeny as well as photochemical and structural properties of a set of bacterial "short" LOV proteins. Specifically, we present evidence of a subclassification of bacterial "short" LOV proteins with respect to conserved sequence features and phylogeny. Five "short" LOV proteins of the Pseudomonadaceae group were spectroscopically characterized, suggesting an evolutionary conservation of fast- and slow-reverting "short" LOV proteins in Pseudomonadaceae. The conservation of N- and C-terminal auxiliary structural elements (Jα-helix and N-cap, respectively) was studied by CD and solution nuclear magnetic resonance (NMR) spectroscopy. Truncation studies conducted with PpSB1-LOV and PpSB2-LOV proteins, as the structural prototypes of the here identified Pseudomonadaceae "short" LOV protein family, suggested that both structural elements contribute to proper protein folding in solution. While bioinformatic sequence analyses of the C-terminal Jα-helix extensions imply the presence of coiled-coil interaction motifs in all Pseudomonadaceae "short" LOV proteins, CD and NMR spectroscopic studies revealed that the respective Jα-helix extensions of PpSB1-LOV and PpSB2-LOV can form independently folding helical structures, but not coiled coils when studied as synthetic peptides in isolated form. Implications for the role of the respective extensions in "short" LOV signaling and for the design of LOV-based optogenetic tools are discussed.

MATERIALS AND METHODS

Bacterial Strains and Plasmids. All bacterial strains used in this study were grown either in Luria-Bertani (LB) broth or in autoinduction (AI) medium[27] as described previously.[25,26] Synthetic genes encoding five Pseudomonadaceae "short" LOV proteins were obtained from Eurofins MWG operon GmbH (Ebersberg, Germany). The respective UniProt entries were as follows: Q3KHW7 for *Pseudomonas fluorescens* Pf0-1-LOV, Q4KI48 for *P. fluorescens* Pf5-LOV, C3K1W0 for *P. fluorescens* SBW25-LOV, B1JAC4 for *P. putida* W619_1-LOV, and B1J385 for *P. putida* W619_2-LOV. The latter organism, like *P. putida* KT2440, possesses two "short" LOV paralogs. All other *Pseudomonas* strains contain only one "short" LOV protein-encoding gene. All genes were custom synthesized carrying 5′-*Nde*I and 3′-*Xho*I restriction endonuclease sites. During gene synthesis, codon usage was not optimized, retaining the original DNA sequence as found in the UniProt and NCBI GenBank databases. *Nde*I and *Xho*I restriction sites were used to subclone the synthetic genes (supplied in a pCR2.1 vector) into pET28a vectors (Novagen/Merck, Darmstadt, Germany) for heterologous expression in *Escherichia coli*. Truncated PpSB1-LOV and PpSB2-LOV constructs were amplified via polymerase chain reaction (PCR) as described below and similarly cloned into the pET28a vector system for expression. All constructs were expressed as N-terminal hexahistidine-tagged fusion proteins (tag sequence, MGSSHHHHHHSSGLVPRGSH) in *E. coli* BL21(DE3). Please note that in this study a PpSB2-LOV construct was used, which in contrast to the database entry (Swiss-Prot entry Q88JB0) lacks the first three N-terminal amino acids.[28] The sequences of all synthetic genes as well as of the truncated PpSB1-LOV and PpSB2-LOV variants were verified by sequencing (SeqLab GmbH, Göttingen, Germany).

General Molecular Biology Techniques. Isolation of recombinant plasmids, gel extraction of DNA fragments, DNA ligation, and transformation of *E. coli* strains were conducted according to standard laboratory protocols.[29]

Construction of Truncated PpSB1-LOV and PpSB2-LOV Variants. The truncated PpSB1-LOV and PpSB2-LOV variants were amplified by PCR from pET28a vectors containing the full-length PpSB1-LOV and PpSB2-LOV coding genes[25,26] by using gene specific primers (Table 1 of the Supporting Information), designed to allow directional cloning of the respective truncated variant into the pET28a vector system by employing 5′-*Nde*I and 3′-*Xho*I restriction endonuclease sites. At the 3′-end of the respective gene fragment, a TAA stop codon was added. The truncated constructs consisted of the following protein segments: PpSB1-ΔNcap (residues 17−142), PpSB1-ΔJα (residues 1−119), PpSB1-ΔNcapΔJα (residues 17−119), PpSB2-ΔNcap (resi-

dues 17−148), PpSB2-ΔJα (residues 1−119), and PpSB2-ΔNcapΔJα (residues 17−119).

Protein Overexpression and Purification. All LOV proteins were expressed and purified using immobilized metal affinity chromatography (IMAC) as described previously.[26] After elution from the IMAC column, the pooled LOV protein-containing fractions were desalted using a Sephadex G25 column. Samples were concentrated employing a VivaSpin concentrator unit (10 kDa molecular mass cutoff) (Sigma-Aldrich, St. Louis, MO). The final buffer was 10 mM sodium phosphate buffer (pH 8.0) supplemented with 10 mM NaCl. All purified proteins were stored at 4 °C in the dark until further use.

Sodium Dodecyl Sulfate−Polyacrylamide Gel Electrophoresis (SDS−PAGE) and Immunoblot Analysis. SDS−PAGE was performed by using 15% polyacrylamide Tris/glycine gels as described by Laemmli,[30] in a vertical MiniProteanII gel apparatus (Bio-Rad Laboratories, Munich, Germany), or by using precast Novex Tris/glycine gels (4−12% polyacrylamide) in an XCell SureLock mini-cell electrophoresis system (Novagen/Merck, Darmstadt, Germany). For SDS−PAGE analyses of soluble and insoluble cell fractions, equal amounts of cells were resuspended [10% (w/v) wet cells] in 10 mM sodium phosphate buffer (pH 8.0) supplemented with 10 mM NaCl. Cells were lysed by being passed three times through a chilled 40K French pressure cell (Thermo Scientific, Waltham, MA) at a constant pressure of 5.5×10^7 Pa. The soluble protein was separated from cell debris and insoluble aggregates by centrifugation at 12000 rpm for 20 min at 4 °C. The resulting supernatant is termed the soluble protein fraction. The insoluble pellet was resuspended in the initial volume of buffer and designated as the insoluble fraction. The protein concentration of the soluble fraction was determined using the Bradford assay.[31] For SDS−PAGE analyses, approximately 20 μg of soluble protein as well as the corresponding volume of the insoluble fraction was loaded per lane.

For Western blot analyses, SDS−PAGE-separated proteins were electro-transferred onto a polyvinylidene fluoride (PVDF) membrane (Bio-Rad Laboratories, Hercules, CA). For the detection of membrane-bound PpSB1-LOV and PpSB2-LOV proteins, polyclonal PpSB1-LOV and PpSB2-LOV antisera (rabbit) (Eurogentec, Seraing, Belgium) were used. For hybridization, antisera were diluted 1:40000 with TBS-T buffer [25 mM Tris-HCl, 3 mM KCl (pH 8.0), and 140 mM NaCl supplemented with 0.2% Tween 20]. As a loading control, T7 RNA polymerase was detected using monoclonal T7 RNA polymerase antibodies (Novagen/Merck) at a 1:20000 dilution in TBS-T. As secondary antibodies, either a goat anti-rabbit horseradish peroxidase (HRP) conjugate (PpSB1-LOV and PpSB2-LOV detection) or a goat anti-mouse HRP conjugate (T7 detection) (Bio-Rad Laboratories, Munich, Germany) was used. Both secondary antibodies allow the detection of the PVDF membrane-bound target antigen by chemiluminescence. Chemiluminescence signals were detected using the Amersham ECL Western Blotting Detection Reagents (GE Healthcare, Uppsala, Sweden) by photographing the blot membrane using a Stella camera system (raytest GmbH, Straubenhardt, Germany).

Peptide Synthesis. PpSB1-Jα (residues 120−142 of the full-length protein) and PpSB2-Jα peptides (residues 120−148 of the full-length protein) were purchased in N-acetylated custom-synthesized form (98% pure) from Peptide 2.0 Inc. (Chantilly, VA): PpSB1-Jα (ACE-S_{120}-RQVELERELAELRAR-PKPDERA_{142}) and PpSB2-Jα (ACE-T_{120}AQVFAEERVRELE-AEVAELRRQQGQAKH_{148}). For NMR or CD analyses, the respective peptides were resuspended to a final concentration of 1 mM in either 100 mM sodium phosphate buffer (pH 6.3) supplemented with 50 mM NaCl or 20 mM sodium phosphate buffer (pH 7.5) supplemented with 1 mM NaCl, respectively.

UV−Vis Absorbance Spectroscopy. All spectroscopic work was conducted under dim red safety light. Light-dependent absorption changes in the UV−vis region (200−600 nm) were recorded using a Beckmann UV650 spectrophotometer (Beckmann Coulter, Krefeld, Germany) with the temperature control set to 37 °C. Protein samples were diluted in 10 mM sodium phosphate buffer supplemented with 10 mM NaCl (pH 8.0). The same buffer was used as a reference. LOV protein light state UV−vis spectra were recorded after illuminating the sample for 30 s using a blue light-emitting Led-Lensers V8 lamp (Zweibrüder Optoelectronics, Solingen, Germany). Dark state recovery was measured from illuminated samples by monitoring the absorption recovery at 480 nm. All dark recovery kinetic measurements were taken three times using three independent protein preparations. Dark recovery time traces were fit using a single-exponential decay function by employing Origin 7G (OriginLab Corp., Northampton, MA).

Circular Dichroism (CD) Experiments. Far-UV circular dichroism (CD) spectra were recorded using a temperature-controlled JASCO J-810 spectropolarimeter. For secondary structure composition analyses, all LOV protein samples [diluted in 10 mM sodium phosphate buffer (pH 8.0) supplemented with 10 mM NaCl] were incubated for 10 min at 20 or 1 °C in the spectropolarimeter. CD spectra were collected between 190 and 250 nm in 0.5 nm intervals with a scan speed of 100 nm/min. Three spectra were averaged to obtain the final CD spectrum of the respective protein. All protein CD spectra were evaluated and deconvoluted using the Convex-Constraint Analysis (CCA) tool by employing a data set of five pure components for the *Pseudomonas* LOV proteins as described previously.[32]

CD Spectroscopic Analysis of Peptide Unfolding and/or Refolding. To monitor the temperature-dependent unfolding of the PpSB1-Jα and PpSB2-Jα peptides, far-UV CD spectra were recorded sequentially while the temperature of the sample was increased from 1 to 65 °C using a constant ramp rate of 1 °C/min. Refolding of the respective peptide was followed in a similar manner by cooling the completely unfolded peptide sample to 1 °C using the same ramp rate. Jα-peptide CD spectra were analyzed as described for the protein samples, but assuming the presence of only two pure components (random coil and α-helix). Melting temperatures were obtained from the plot of the ellipticity at 222 nm (Θ_{222}) versus temperature (Figure 5) by fitting the experimental data to eq 1. The same fit was used to estimate the maximal and minimal ellipticity values for the fully folded peptides, $[\Theta]_{folded}$, and the completely unfolded peptides, $[\Theta]_{unfolded}$. Those latter values were used to quantitatively describe α-helix melting in terms of the α-helical fraction (f_α) under the premise of a two-state transition (eq 2).

$$\Theta_{222}(T) = \frac{[\Theta]_{folded} - [\Theta]_{unfolded}}{1 + e^{(T-T_m)/dx}} + [\Theta]_{unfolded} \quad (1)$$

$$f_\alpha = \frac{[\Theta] - [\Theta]_{unfolded}}{[\Theta]_{folded} - [\Theta]_{unfolded}} \quad (2)$$

Thermodynamic parameters were obtained by fitting the calculated equilibrium α-helix fraction (f_α) to eq 3

$$\ln(K_{eq}) = \ln\left(\frac{f_\alpha}{1-f_\alpha}\right) = \frac{-\Delta H}{R}\left(\frac{1}{T}\right) + \frac{\Delta S}{R} \quad (3)$$

The fits of $\ln(K_{eq})$ versus $1/T$ were highly linear with R values of >0.999. From this fit, values for enthalpy ΔH and entropy ΔS were obtained. The relation $\Delta G = \Delta H - T\Delta S$ was used to obtain the Gibbs free energy of unfolding (ΔG) at a given temperature.

NMR Experiments. All NMR measurements were taken in 100 mM sodium phosphate buffer (pH 6.3) supplemented with 50 mM NaCl, deuterated 2,2,2-trifluoroethanol (TFE) with a final concentration of 10% (v/v) (PpSB1-Jα) or 25% (v/v) (PpSB2-Jα), and 10% (v/v) D_2O. Lyophilized peptide samples were dissolved in the buffer described above to a final concentration of ~1 mM. All NMR experiments were conducted at 25 °C using 5 mm Shigemi NMR tubes on a Varian VNMRS 900 MHz NMR spectrometer equipped with a Z-axis pulsed-field-gradient triple-resonance cryo-probe. Experimental data were collected in phase-sensitive mode using quadrature detection in ω_1 by time-proportional phase incrementation. The water signal was suppressed by the WATERGATE method. Resonance assignment for both peptide samples was accomplished using two-dimensional (2D) (^{1}H−^{1}H) TOCSY and (^{1}H−^{1}H) NOESY experiments. A mixing time of 60 ms and a B1 field of 9000 Hz were used for 2D ^{1}H−^{1}H TOCSY experiments. 2D ^{1}H−^{1}H NOESY experiments were performed with a mixing time of 350 ms. All 2D spectra were collected acquiring 256 increments in the F_1 dimension each consisting of 80 scans. ^{1}H chemical shifts were referenced externally to 2,2-dimethyl-2-silapentane sulfonate at 0 ppm.

Structure Calculations and Structure Analysis. Time domain NMR data were processed and converted into the frequency domain with the aid of NMRPipe.[33] Spectral evaluation and proton resonance assignment were conducted using CcpNmr Analysis.[34] NOESY cross-peak assignment and structure calculations were performed using the combination of Aria version 2.3.1[32] and CNS version 1.21[35,36](including the Aria patchset) with the PARALLHDG version 5.3 force field. All MD parameters were used in the default configuration, but the numbers of steps were increased to 8000 during refinement and 20000 in each cooling phase. The 10 lowest-energy structures of the 250 calculated were further refined in explicit water as a final step in the Aria procedure. Geometrical parameters of the derived structural models and the corresponding secondary structure distribution were analyzed and visualized using MOLMOL,[37] PyMOL,[38] WHAT-IF,[39] and MolProbity.[40] The residue-wise secondary structure propensity (SSP) for the peptide samples was estimated from NMR chemical shift data using the SSP tool developed by Marsh and co-workers.[41] For the superposition and analysis of structures, either PyMOL (Schrödinger LLC, Cambridge, MA)[38] or the Yasara structure suite[42] was employed.

Bioinformatic Analysis. Initially, protein sequences that were significantly similar to the two "short" LOV proteins of *P. putida* KT2440 were obtained from the NCBI database by using the PSI-BLAST tool[43] employing the PpSB1-LOV and PpSB2-LOV amino acid sequences as a query. To verify coverage of all Pseudomonadaceae genome sequences, the same search was conducted using the NCBI genomic group BLAST tool (http://www.ncbi.nlm.nih.gov/sutils/genom_table.cgi), restricting the search to the group of Pseudomonadaceae. Domain content analyses were performed using the SMART tool.[44] Amino acid sequence alignments were generated with T-COFFEE.[45] Alignments were visualized and edited manually using GeneDoc.[46] Bootstrapped maximum-likelihood trees with 100 replicates for each run were generated using the RaxML webserver.[47] Sequence IDs as well as accession numbers for the respective protein sequences can be found in Table 2 of the Supporting Information. The multiple-sequence alignment used for phylogenetic tree computations is shown in Figure 1 of the Supporting Information. The PCOILS webserver[48] was used to analyze Jα-helix sequences for the presence of a coiled-coil heptad repeat pattern. Residue-wise charges and average hydropathies (according to the Kyte−Doolittle scale[49]) were inferred from sequence alignments using custom Perl scripts.

RESULTS

Distribution and Phylogeny of "Short" LOV Proteins in Prokaryotes. To elucidate the "short" LOV protein distribution and phylogeny in more detail, we obtained sequences that were significantly similar to PpSB1-LOV and PpSB2-LOV from GenBank. To verify all obtained sequences are part of the "short" LOV protein family, we performed domain content analyses using the SMART webserver.[44] In this way, we obtained 61 sequences from 53 different bacteria (Table 2 of the Supporting Information). With the exception of one sequence from the actinobacterium *Nakamurella multipartita* Y-104, "short" LOV protein sequences are apparently present only in proteobacteria. In proteobacteria, they are predominant in the γ-subclass (38 sequences) and α-subclass (18 sequences) and can be found in a limited subset of β-proteobacteria (4 sequences). The corresponding phylogentic tree suggested the separation into γ-proteobacterial "short" LOV proteins (Figure 1, colored dark blue, green, light blue, and black) and "short" LOV proteins of other proteobacteria (Figure 1, colored gray). A closer look into the sequence diversity present in the respective alignment (Figure 1 of the Supporting Information) further supports this subdivision by revealing a previously noted noncanonical FMN-binding motif, Y(Q/R)D<u>C</u>RFLQG, for most γ-proteobacterial "short" LOV sequences (Figure 1 of the Supporting Information). The remaining "short" LOV proteins contained the classical G(X)N<u>C</u>RFLQG motif present in all other prokaryotic and eukaryotic LOV proteins (Figure 1 of the Supporting Information).

In particular, all "short" LOV sequences of the Pseudomonadaceae group (24 sequences) contain the noncanonical Y(Q/R)DCRFLQG sequence motif. Among those, 12 organisms possess only one "short" LOV homologue, whereas six organisms that contain, like *P. putida* KT2440, two genes encoding "short" LOV proteins can be identified. Currently, the Pseudomonadaceae group comprises 181 unique strains for which the genome is completely sequenced. Given this number, "short" LOV proteins with a high level of sequence similarity and thus probably structural and functional similarity to the two *P. putida* KT2440 "short" LOV proteins can be found in ~10% of the sequenced Pseudomonadaceae. The only other γ-proteobacterial orders in which "short" LOV protein sequences, comprising the Y(Q/R)DCRFLQG signature motif, can be identified are Oceanospirillales, Chromatiales, and Thiotrichales.

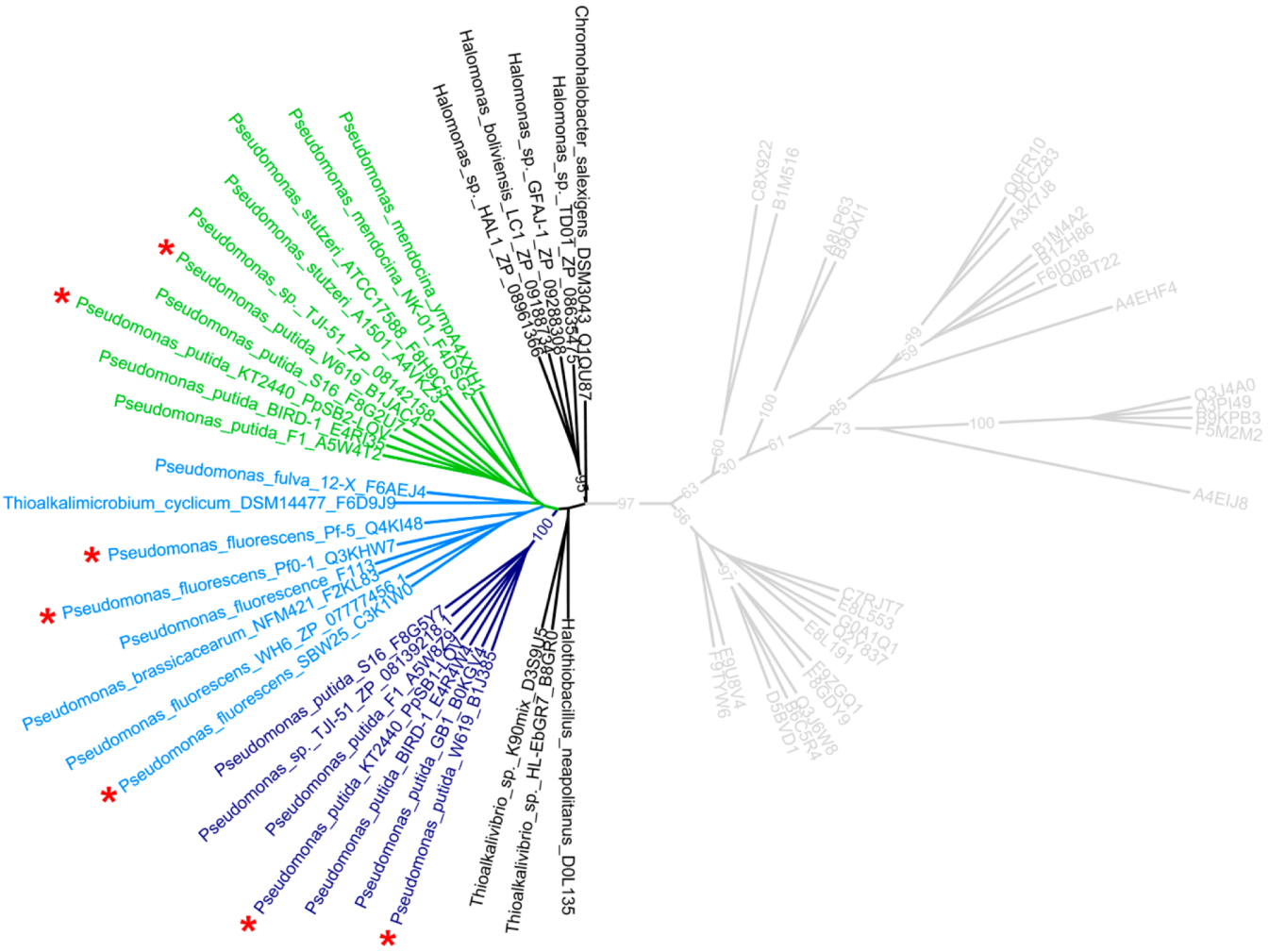

Figure 1. Unrooted phylogentic tree illustrating the distribution and evolutionary divergence of "short" LOV proteins. The tree can globally be divided into two parts: (i) sequences of γ-proteobacterial origin comprising the noncanonical Y(Q/R)DCRFLQG FMN-binding motif (colored black, dark blue, light blue, and green) and (ii) sequences of other proteobacterial subclasses comprising the canonical LOV protein motif G(X)NCRFLQG (colored gray). In the γ-proteobacterial branch, the two *P. putida* KT2240 "short" LOV proteins, PpSB1-LOV and PpSB2-LOV, are found on two distinct clades. The PpSB1-LOV clade is colored dark blue and the PpSB2-LOV clade green. Whereas the PpSB1-LOV clade (dark blue) is comprised solely of *P. putida* sequences, sequences of *P. mendocina* and *P. stutzeri* strains can be found in the PpSB2-LOV clade (green). A third clade (light blue) is formed by sequences from *P. fluorescens*, *P. cyclicum*, and *P. fulva* strains. "Short" LOV sequences from organisms outside the Pseudomonadaceae group are found in orders Oceanospirillales, Chromatiales (black), and Thiotrichales (*T. cyclicum* strain DSM14477, light blue). The Pseudomonadaceae "short" LOV proteins that were characterized in this study are denoted with red asterisks.

In the γ-proteobacterial branch, the two *P. putida* KT2240 "short" LOV proteins, PpSB1-LOV and PpSB2-LOV, are found on three distinct clades (Figure 1). Whereas the PpSB1-LOV clade (Figure 1, dark blue) is comprised solely of *P. putida* sequences, sequences of *Pseudomonas mendocina* and *Pseudomonas stutzeri* strains can be found in the PpSB2-LOV clade (Figure 1, green). A third clade (Figure 1, light blue) is formed by "short" LOV sequences from *P. fluorescens*, *Pseudomonas cyclicum*, *Pseudomonas fulva*, and *Thioalkalimicrobium cyclicum*. The latter sequence represents an exception as it, as a sequence of Thiotrichales origin, clusters within the Pseudomonadaceae clade. Please note that this grouping is incongruent with general organismal phylogeny as reconstructed from 16s rRNA sequences and thus highlights the possibility of "short" LOV inheritance via horizontal gene transfer. Two additional distinct clades are formed by sequences originating from Oceanospirillales (e.g., *Chromohalobacter salexigens* DSM 3043) and Chromatiales (e.g., *Halothiobacillus neapolitanus*) (Figure 1, black).

UV−Vis Spectroscopic and Biochemical Characterization of an Exemplary Set of Pseudomonadaceae "Short" LOV Proteins. The clear separation of the fast-reverting PpSB2-LOV protein sequence from its slow-reverting PpSB1-LOV counterpart on two distinct clades in the phylogentic tree suggests an evolutionary conservation of fast- and slow-reverting "short" LOV proteins in the Pseudomonadaceae group. To study the conservation of structural features and recovery kinetic properties, we cloned, expressed, purified, and characterized a set of five different "short" LOV proteins found in the three distinct Pseudomonadaceae clades. The following "short" LOV proteins were selected as representative sequences: *P. fluorescens* Pf01-LOV (Q3KHW7), *P. fluorescens* Pf5-LOV (Q4KI48), *P. fluorescens* SBW25-LOV (C3K1W0), *P. putida* W619_1-LOV (B1JAC4), and *P. putida* W619_2-LOV (B1J385). All five sequences show the classical features of the Pseudomonadaceae "short" LOV protein family, i.e., Y(Q/R)D<u>C</u>RFLQG motif, conserved N-cap, and C-terminal Jα-extension. All proteins could be expressed in soluble form in *E.*

dx.doi.org/10.1021/bi400311r | *Biochemistry* 2013, 52, 4460−4473

coli and were purified to homogeneity as described previously for PpSB1-LOV and PpSB2-LOV.[25] After equilibration for 2 days at 4 °C in the dark, all protein samples were visibly yellow, indicating the presence of a noncovalently bound flavin chromophore. All five proteins appeared to be dimeric in high-performance liquid chromatography (HPLC)-based size-exclusion chromatographic studies (Table 3 of the Supporting Information). HPLC analyses of the chromophore content revealed that all proteins bound predominately FMN as well as a certain amount of riboflavin as a chromophore (Table 3 of the Supporting Information). With respect to quaternary structure and flavin chromophore content, all of the studied proteins were thus highly similar to the two previously characterized *P. putida* KT2440 LOV proteins.[25] Dark state and photoequilibrium (30 s of blue light illumination) UV−vis spectra are depicted in Figure 2. All proteins displayed typical phototropin LOV-like UV−vis spectral characteristics as well as blue light sensitivity (Figure 2).

Much to our surprise, for two of the five proteins, namely, Pf01-LOV and SBW25-LOV, no recovery was observed from photoequilibrium to the dark state after illumination with blue light. Hereby, when measured at 25 °C, next to no spectral recovery of the flavin specific absorption band in the blue region of the spectrum (400−500 nm) was visible over 16 h of measuring time (data not shown). One possible explanation to account for such a behavior would be a very slow dark recovery reaction, even beyond that of the already slow-reverting PpSB1-LOV protein (τ_{rec} of ∼2400 min at 25 °C[25]). Consequently, we attempted to accelerate the thermal breaking of the covalent FMN-C4a-cysteinyl-thiol adduct by conducting measurements at 37 °C. At this temperature, full recovery could be achieved for the two very-slow-reverting proteins. For comparison, we also recorded dark recovery time traces for the two previously studied *P. putida* KT2440 "short" LOV proteins at 37 °C. The adduct state lifetimes (τ_{rec}) of the four *P. putida* (strains KT2440 and W619) proteins were as follows: 109 ± 18 min for PpSB1-LOV, 0.5 ± 0.1 min for PpSB2-LOV, 53 ± 4 min for W619_1-LOV, and 0.9 ± 0.1 min for W619_2-LOV. Even at this elevated temperature, both *P. fluorescens* proteins displayed a very slow dark recovery with τ_{rec} values of 810 ± 72 min for Pf01-LOV and 1470 ± 100 min for SBW25-LOV. Please note that for the latter protein dark recovery time traces could not be measured until reversion was complete because of the inherent instability of the protein over the extended measuring times at 37 °C. During the measurement, SBW25-LOV partially precipitates and loses the FMN chromophore, complicating interpretation of the data. Thus, the presented adduct state lifetime represents only a lower bound estimate. Compared to the slow-reverting PpSB1-LOV protein, Pf0-1-LOV and SBW25-LOV revert 7 and 13 times slower, respectively. Surprisingly, Pf5-LOV displayed an adduct state lifetime (τ_{rec}) of ∼3.6 ± 1.5 min and is thus rather fast-reverting.

Bioinformatic Analysis of N- and C-Terminal Extension of the Pseudomonadaceae "Short" LOV Protein Family. The N-terminal region, corresponding to the N-cap (helix A′α) of PpSB1-LOV, is conserved in sequence in all γ-proteobacterial "short" LOV proteins (Figure 1 of the Supporting Information). In contrast, the C-terminal extension (Jα-helix) is much more variable in both length and sequence. The recently determined crystal structure of PpSB1-LOV [Protein Data Bank (PDB) entry 3SW1][7] revealed that both auxiliary structural elements are part of the subunit interface stabilizing the formation of the parallel homodimer in the

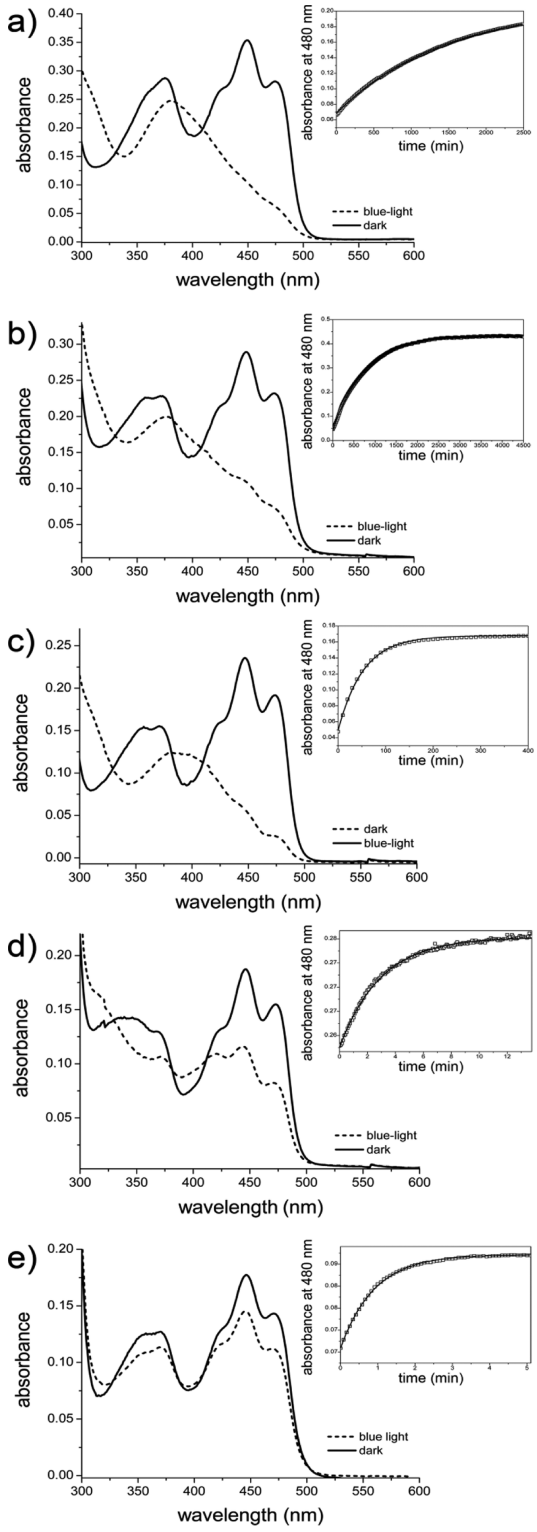

Figure 2. Blue light sensitivity of Pseudomonadaceae "short" LOV proteins. UV−vis absorbance spectra of the dark state (—) and the respective photoequillibrium state recorded after illumination with blue light for 30 s (---). The inset shows the respective dark recovery time traces recorded at 480 nm absorbance. All measurements were performed at 37 °C. The adduct state lifetimes (τ_{rec}), determined from single-exponential fits of the experimental data, were as follows: (a) 1470 ± 100 min for SBW25-LOV, (b) 810 ± 72 min for Pf01-LOV, (c) 53 ± 4 min for W619_1-LOV, (d) 3.6 ± 1.5 min for Pf5-LOV, and (e) 0.9 ± 0.1 min for W619_2-LOV.

dx.doi.org/10.1021/bi400311r | *Biochemistry* 2013, 52, 4460−4473

crystal mostly via hydrophobic interchain contacts. The C-terminal Jα-helix, which protrudes from the LOV core, hereby supports subunit association via a coiled-coil-like arrangement of interface-buried hydrophobic residues. To verify whether this structural feature might be conserved in all Pseudomonadaceae "short" LOV proteins, we analyzed the respective protein sequences for the presence of the canonical *abcdefg* heptad repeat pattern characteristic of coiled-coil structures (Figure 3).

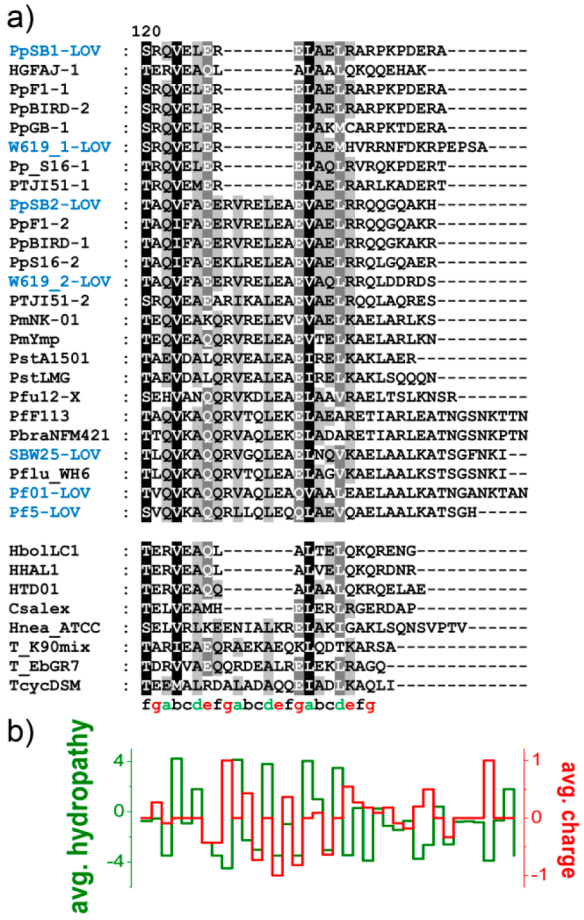

Figure 3. Sequence alignment of the C-terminal Jα-helix extensions of Pseudomonadaceae "short" LOV proteins (a) and average hydropathies as well as average charges inferred from the alignment (b). Average residue-wise hydropathies were assigned according to the Kyte–Doolittle scale.[49] Jα-helix sequences highlighted in blue denote "short" LOV proteins that were experimentally characterized in this study.

For all sequences, the coiled-coil prediction tool PCOILS[48] predicts the presence of either two or three heptad repeats (Figure 3a). This is also apparent in the alignment (Figure 3a) where two distinct sequence length patterns can be identified. In a subset of sequences, a conserved seven-amino acid insertion is present after the first heptad repeat, accounting for two helical turns in structure. Moreover, the structural interaction pattern typical for coiled coils, featuring hydrophobic interactions via residues *a*–*d* and salt bridge contacts via residues *e*–*g* of the heptad, is conserved in all sequences (Figure 3b). Thus, bioinformatic analyses for sequences of the Pseudomonadaceae "short" LOV family suggest the presence of a well-defined N-cap as well as C-terminal Jα-helix elements prone to mediating subunit association via coiled-coil interactions, much like in the PpSB1-LOV crystal structure.

CD Spectroscopic Studies of the Pseudomonadaceae "Short" LOV Proteins. To assess the global secondary structure content of the five new Pseudomonadaceae "short" LOV proteins, we conducted CD spectroscopic studies in a manner similar to that described for PpSB1-LOV and PpSB2-LOV.[25] Far-UV CD spectra recorded at 20 °C were used to estimate the secondary structure content of the five LOV proteins. CD spectra were deconvoluted using the convex constraint analysis tool (CCA+)[50] applying a data set of five pure components: (i) α-helices, (ii) turns and other structures, (iii) parallel and twisted β-sheets, (iv) random coils, and (v) antiparallel β-sheets.[25,51] Table 1 summarizes the CCA-derived secondary structure content of the five Pseudomonadaceae "short" LOV proteins in comparison to that of PpSB1-LOV and PpSB2-LOV.[25]

Table 1. Results of the CCA Analysis of CD Spectra

protein	no. of residues/length of Jα-helix	CD-derived secondary structure content,[a] no. of amino acids		
		α-helix	β-strands	coil, turn, other
PpSB1-LOV	162/23	47 ± 3	44 ± 4	71 ± 3
W619_1-LOV	166/27	44 ± 1	45 ± 4	77 ± 5
Pf01-LOV	178/38	57 ± 7	41 ± 2	80 ± 9
SBW25-LOV	175/36	69 ± 7	35 ± 8	71 ± 1
PpSB2-LOV	168/29	45 ± 1	54 ± 1	71 ± 5
W619_2-LOV	168/29	44 ± 2	54 ± 4	70 ± 2
Pf5-LOV	172/33	60 ± 1	42 ± 1	70 ± 1
PDB entry 3SW1[b]	134/15	53	46	35

[a]For PpSB1-LOV and PpSB2-LOV, values are derived from three CD measurements of three independent preparations.[25,26] For all other proteins, two measurements of two independent preparations were used for spectral deconvolution using the CCA+ tool.[50] For deconvolution, a set of five pure components was used as described previously.[25,51] [b]Secondary structure content derived from the crystal structure of full-length PpSB1-LOV.[7] The first 20 amino acids comprising the N-terminal His tag and a thrombin cleavage site as well as the last 12 C-terminal amino acids are lacking electron density in the crystal structure and are thus likely disordered.[7] This accounts for the difference between the CD-derived random coiled content of PpSB1-LOV in solution and the value derived from analysis of the crystal structure.

All studied "short" LOV proteins display very similar β-strand/turn and random-coil content. However, significant differences are found in their α-helix content. In particular, for the proteins with a longer C-terminal extension (Pf01-LOV, SBW25-LOV, and Pf5-LOV), the CD-derived α-helix content is increased compared to that of PpSB1-LOV.

Effect of N- and C-Terminal Truncations on the Soluble Expression of PpSB1-LOV and PpSB2-LOV in *E. coli*. To gain more insight into the structural role of the N-terminal cap (N-cap) and the C-terminal Jα-helix present outside the LOV core domain in the Pseudomonadaceae "short" LOV protein family, we generated a set of truncated protein variants of the two prototype proteins PpSB1-LOV and PpSB2-LOV. Using molecular biological means, constructs were generated lacking either the N-cap (ΔNcap), the Jα-helix (ΔJα), or both structural elements (ΔNcap-ΔJα). All constructs were expressed in *E. coli* in a manner identical to

dx.doi.org/10.1021/bi400311r | *Biochemistry* 2013, 52, 4460–4473

that of the corresponding full-length proteins. Cells were lysed, and insoluble material was separated by centrifugation. The resulting protein fractions (insoluble pellet and soluble protein-containing supernatant) were separated by SDS−PAGE and transferred to a PVDF membrane. The respective LOV protein was detected immunologically using polyclonal antisera raised against either PpSB1-LOV or PpSB2-LOV (Figure 4). This

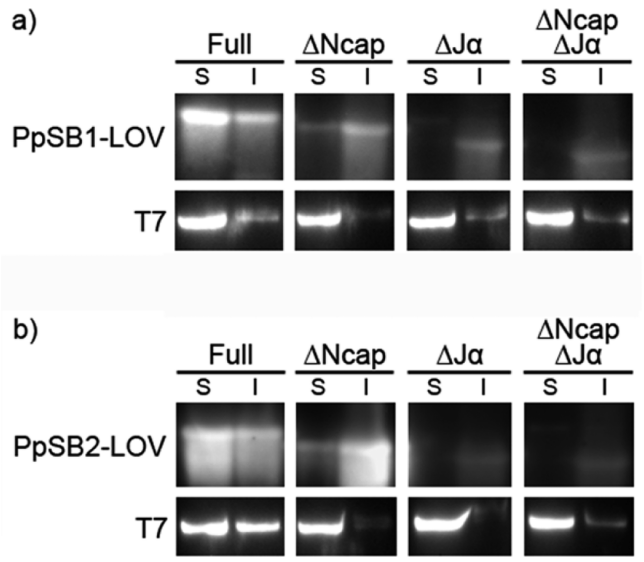

Figure 4. Immunoblot analysis illustrating the effect of N-terminal (N-cap) and C-terminal (Jα-helix) truncations of PpSB1-LOV (a) and PpSB2-LOV (b) on the accumulation of soluble and insoluble LOV protein in *E. coli* BL21(DE3). The respective full-length genes (Full), the N-terminally truncated construct (ΔNcap), the C-terminally truncated construct (ΔJα), and constructs lacking both structural elements (ΔNcapΔJα) were expressed using autoinduction medium in *E. coli* BL21(DE3) under identical conditions. After cell lysis, the soluble protein was separated from protein aggregates, inclusion bodies, and cell debris by centrifugation. Similar amounts of the resulting soluble (S) and insoluble (I) protein fraction were analyzed by immunoblotting. As a loading control, T7 RNA polymerase was expressed in *E. coli* BL21(DE3) by autoinduction and quantified in soluble and insoluble fractions.

strategy allows specific detection of even trace amounts of both proteins and the corresponding variants. Much to our surprise, removal of either structural element severely compromised the soluble expression of the respective truncated variants (Figure 4).

Whereas both full-length proteins are present predominately in the soluble fraction (solubility of ≥60%), removal of the N-cap results in an increased level of accumulation of the respective variants in the form of insoluble aggregates (solubility of ≤20%). Removal of the C-terminal Jα-helix or of both the N-cap and the Jα-helix has a much more detrimental effect on the production of the soluble protein. The respective truncated constructs accumulated exclusively in the form of insoluble aggregates; no soluble protein was detectable. As a loading control, T7 RNA polymerase (T7Pol) was quantified in the soluble and insoluble fractions after lactose-induced expression of the *T7pol* gene in *E. coli* BL21(DE3) (Figure 4a,b, bottom panels). In the autoinduction expression system employed here, *T7pol* gene expression was induced depending on growth and the metabolic state of the cell.[52] Hereby, depletion of glucose and the onset of utilization of lactose and/or glycerol resulted in T7 RNA polymerase gene expression from the lactose-inducible P_{lacUV5} promoter, which in turn facilitates target gene expression under control of the strong P_{T7} promoter. All samples of the soluble cell fraction contained very similar amounts of T7 RNA polymerase, thus verifying similar loading levels for the respective soluble samples (Figure 4). Please note that T7Pol is usually expressed in soluble form in *E. coli* BL21(DE3). Thus, T7Pol signals seen in the insoluble fraction most probably arise from the presence of a certain fraction of aggregated protein and/or incomplete cell lysis. We subsequently tried to purify both N-cap truncated variants of PpSB1-LOV and PpSB2-LOV as a small but detectable amount of soluble protein could be obtained. We were able to obtain milligram amounts of the purified protein, which however lacked bound FMN or rapidly lost the chromophore during desalting and concentration steps (data not shown). Taken together, the data indicate that removal of both auxiliary structural elements outside the LOV core (N-cap and Jα-helix) severely compromises the structural integrity of the two studied "short" LOV proteins.

Far-UV CD Spectroscopy To Probe Thermal Unfolding of the PpSB1-Jα and PpSB2-Jα Peptides. Coiled coils are widespread, many times independently folding, interaction motifs present in many structurally different proteins.[53] Therefore, we asked the question of whether the Jα-helix extension of PpSB1-LOV and PpSB2-LOV can fold in a manner that is independent of the rest of the protein. Given the short length of the Jα-helix extensions, we obtained both protein segments (PpSB1-Jα and PpSB2-Jα) as custom-synthesized N-terminally acetylated peptides.

To study the folding and secondary structure of both peptides, we used far-UV CD spectroscopy. Initially, CD spectra were recorded at 20 °C. At this temperature, clear spectral evidence of the presence of α-helical secondary structure could be obtained for only PpSB2-Jα (data not shown). Therefore, spectra were recorded at 1 °C and deconvoluted assuming the presence of two pure components (α-helix and random coil). The CD-predicted secondary structure content of the two peptides at 1 °C is given in Table 2. The far-UV CD spectra used for deconvolution are depicted in Figure 2 of the Supporting Information (black line). At 1 °C, both peptides are partially α-helical with 41 and 56% α-helical content for PpSB1-Jα and PpSB2-Jα, respectively. We studied thermal unfolding by collecting CD spectra for the two

Table 2. CD Spectroscopic Studies of PpSB1-Jα and PpSB2-Jα

	melting curve-derived thermodynamic parameters[a]			
peptide	T_m (°C)	ΔH (kcal mol^{-1})	ΔS (kcal K^{-1} mol^{-1})	ΔG (kcal mol^{-1})[b]
PpSB1-Jα (23 amino acids)	4	9.3	0.0336	0.26
PpSB2-Jα (29 amino acids)	16	14.3	0.0494	0.87

	CD-derived secondary structure content (%)[b] (no. of amino acids)	
	α-helix	random coil
PpSB1-Jα (23 amino acids)	41 (9)	59 (14)
PpSB2-Jα (29 amino acids)	56 (16)	44 (13)

[a]CD spectra of both peptides were determined in thermal equilibrium. Heating was performed from 1 to 65 °C until complete unfolding had been observed. [b]Derived from spectra recorded at 1 °C.

dx.doi.org/10.1021/bi400311r | *Biochemistry* 2013, 52, 4460−4473

peptide samples equilibrated at 1 °C and subsequently heating the samples stepwise to >65 °C with a constant ramp rate of 1 °C/min. When the samples were heated, a clear loss of negative ellipticity at 222 and 208 nm could be detected, suggestive of the loss of α-helical secondary structure (Figure 2 of the Supporting Information). Eventually, heating results in the formation of a spectral species with a blue-shifted minimum, resembling the CD spectra of random-coil model peptides.[54] The presence of one isodichroic point at 203 nm is supportive of a two-state transition. Interestingly, the thermal unfolding process is fully reversible for both peptides, with both the unfolding and folding transition displaying the same transition behavior (Figure 5). Under the premise of complete reversibility while assuming a two-state transition, thermodynamic parameters for the PpSB1-Jα and PpSB2-Jα unfolding−folding equilibrium can be extracted from CD data[55] (Table 2).

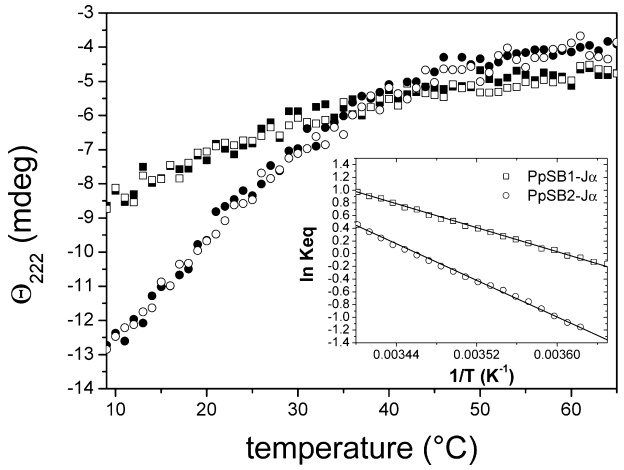

Figure 5. Unfolding (filled symbols) and refolding (empty symbols) curves recorded for PpSB1-Jα (squares) and PpSB2-Jα (circles). The depicted curves were extracted from the respective far-UV CD spectra by plotting Θ_{222} vs incubation temperature. Samples were equilibrated at 1 °C. Subsequently, CD spectra were recorded for the same sample heated stepwise to >65 °C using a constant ramp rate of 1 °C/min. After complete unfolding had been achieved, CD spectra were recorded for the same samples cooled stepwise to 1 °C using the same ramp rate that was used for heating. The inset depicts the van't Hoff plot (eq 3) for the unfolding−refolding transition of PpSB1-Jα (□) and PpSB2-Jα (○) that was used to derive the thermodynamic parameters listed in Table 2.

With an estimated melting temperature (T_m) of 16 °C, PpSB2-Jα appears to be slightly more stable against thermal unfolding than the PpSB1-Jα peptide (T_m = 4 °C). At 1 °C, PpSB1-LOV is marginally stabilized against unfolding with a Gibbs free energy of unfolding (ΔG) of 0.26 kcal mol^{-1} (ΔH = 9.3 kcal mol^{-1}, and ΔS = 0.0336 kcal K^{-1} mol^{-1}). For the thermally more stable peptide, PpSB2-Jα, the Gibbs free energy of unfolding (ΔG) is increased to 0.87 kcal mol^{-1} (ΔH = 14.3 kcal mol^{-1}, and ΔS = 0.0494 kcal K^{-1} mol^{-1}). This renders both isolated Jα peptides rather thermally unstable. However, the data nevertheless prove that both peptides are able to spontaneously adopt α-helical structures even when studied in isolated form in aqueous (buffer) solution.

NMR Solution Structure of the C-Terminal PpSB1-LOV and PpSB2-LOV Jα-Helix Extensions. The structure of both Jα-helix peptides was probed via solution NMR spectroscopy. Initially, 2D ^{1}H−^{1}H TOCSY spectra were collected at 1 °C for both peptides. However, at this temperature, severe line broadening was observed, yielding spectra that could not be interpreted. Spectra recorded at 25 °C were fully resolved. However, at this temperature, both peptides are already partially or completely unfolded. Therefore, we used the helix-stabilizing agent 2,2,2-trifluoroethanol (TFE) to stabilize α-helical peptide conformations at 25 °C. TFE is not a helix-inducing solvent in the sense that it will induce helix formation in a manner independent of the sequence. It is rather a helix-enhancing cosolvent that stabilizes helices in regions with some α-helical propensity.[56] To verify proper folding at 25 °C in the presence of minimal amounts of TFE, we recorded CD spectra for the peptide samples at 25 °C while sequentially increasing the TFE concentration (data not shown). In this way, the minimal concentration of TFE needed to promote complete folding of the respective peptide was determined. For the two peptides, addition of 10% (v/v) TFE (PpSB1-Jα) and 25% (v/v) TFE (PpSB2-Jα) was necessary to stabilize peptide folding at 25 °C. Under those buffer conditions, 2D (^{1}H−^{1}H) TOCSY spectra and 2D (^{1}H−^{1}H) NOESY spectra were recorded for the PpSB1-Jα and PpSB2-Jα peptides. Sequential assignment of the proton resonances was achieved considering sequential $H^N_{(i)}$−$H^N_{(i+1)}$, $H^\alpha_{(i)}$−$H^N_{(i+1)}$, and $H^\beta_{(i)}$−$H^N_{(i+1)}$ NOE correlations. Structures were calculated using CNS by utilizing 537 (PpSB1-Jα) and 749 (PpSB2-Jα) NOE-derived distance restraints, of which 485 (PpSB1-Jα) and 721 (PpSB2-Jα) were unambiguous. Structure quality, distance restraint, and violation statistics for the ensemble of the 10 lowest-energy structures are listed in Table 3.

The final ensemble of 10 structures was selected on the basis of energy from the ensemble of 250 calculated structures and subjected to a refinement in explicit water. The rmsd of the backbone atoms for the refined ensemble from the mean structure was 0.053 Å for PpSB1-Jα (ordered region of residues 121−134) and 0.191 Å for PpSB2-Jα (ordered region of residues 121−142). No NOE violations greater than 0.3 Å were observed. Figure 6 depicts the overlay of the 10 ensemble structures (Cα trace as a ribbon drawing) superimposed over the respective helical portion (as a transparent cartoon).

Please note that NMR structural models derived from NOE-based structure calculations inevitably overestimate the real secondary structure content of the ensemble. To quantify the α-helical secondary structure content directly from NMR chemical shift data, we used the secondary structure propensity score (SSP) developed by Marsh and co-workers.[41] An SSP score at a given residue of 1 or −1 is indicative of fully formed α- or β-structure, respectively. A score of 0.5 indicates that 50% of the conformers in the disordered state ensemble are helical at that position.[41] Figure 3 of the Supporting Information depicts the residue-wise SSP score for PpSB1-Jα (panel A) and PpSB2-Jα (panel B). For both peptides, most residue SSP scores are positive, indicative of a certain degree of α-helical propensity. Exceptions include R135 (PpSB1-Jα) and K147 (PpSB2-Jα), which show negative values. Average SSP scores for the ordered region of PpSB1-Jα (residues 121−134) and PpSB2-Jα (residues 121−142) are 0.48 and 0.44, respectively. This suggests that on average 48 and 44% of the conformers in the respective regions are α-helical in the disordered state ensemble. While SSP scores provide a more realistic measure of the true α-helical propensity of the sample, they unfortunately do not allow a clear-cut estimation of, for example, the percentage of residues in an α-helical conformation. Given the average SSP scores of 0.48 and 0.44 for the ordered region of

dx.doi.org/10.1021/bi400311r | Biochemistry 2013, 52, 4460−4473

Table 3. Structural, Distance Restraint, and Violation Statistics for the 10 Lowest-Energy Structures of PpSB1-Jα and PpSB2-Jα

	PpSB1-Jα (residues 120−142)	PpSB2-Jα (residues 120−148)
no. of experimental restraints		
total NOE distance restraints	537	749
unambiguous	485	721
intraresidue	190	321
interresidue	295	400
sequential	159	195
short range (2−3)	108	157
medium range (4−5)	28	48
long range (>5)	0	0
ambiguous	52	28
no. of NOE upper bound violations		
violations of >0.5 Å	0	0
violations of >0.3 Å	0	0
violations of >0.1 Å	12.1 ± 1.7	19.4 ± 2.0
rmsd from idealized covalent geometry		
bonds (Å)	0.004 ± 0.0001	0.004 ± 0.0001
angles (deg)	0.519 ± 0.0157	0.583 ± 0.0146
impropers (deg)	0.965 ± 0.1498	1.247 ± 0.1199
rmsd from experimental restraints		
NOE restraints (Å)	0.028 ± 0.002	0.027 ± 0.000
Ramachandran plot (ensemble)		
favored region	95.9%	95.4%
allowed region	100%	100%
disallowed region	0%	0%
ensemble rmsd (Å)		
core residues	121−134	121−142
backbone	0.053	0.191
heavy atoms	1.003	0.789

both peptides discussed above, we can set an arbitrary minimum threshold for the propensity of defining a residue in α-helical conformation of ∼0.4. Assuming this arbitrary SSP threshold, 9 of 23 residues for PpSB1-Jα (40%) and 16 of 29 residues for PpSB2-Jα (55%) possess a strong tendency for α-helical secondary structure. This translates roughly to three and five helical turns in structure for PpSB1-Jα and PpSB2-Jα, respectively. Additionally, evidence of the presence of an α-helical conformation of both peptide samples is provided by the observed NOE pattern typical for α-helices (Figure 3 of the Supporting Information).

The numbers of amino acid residues showing chemical shifts and NOE patterns typical for α-helical secondary structure are in good agreement with CD and bioinformatic predictions (Table 2 and Figure 3). Moreover, the CD and NMR data are coherent, as both methods predict that PpSB2-Jα is extended compared to PpSB1-Jα. This is in accordance with alignment analyses, where a conserved seven-residue insertion is observed for a subset of Pseudomonadaceae "short" LOV protein Jα-helix sequences (Figure 3).

DISCUSSION

Phylogenetic Analyses and Mutually Conserved Photocycle Kinetic Parameters Hint at a Conserved Physiological Role of Fast- and Slow-Reverting Pseudomonadaceae "Short" LOV Proteins. A comprehensive sequence database search was performed and a phylogenetic tree inferred from the retrieved sequences to provide a basis for the identification of prokaryotic PpSB1-LOV- and PpSB2-LOV-like "short" LOV proteins. Sequence alignment data (Figure 1 of the Supporting Information) as well as phylogenetic analyses (Figure 1) revealed a division of prokaryotic "short" LOV proteins into at least two subclasses. Hereby, it appears that "short" LOV proteins are solely present in proteobacteria. Sequences bearing the canonical LOV sequence motif G(X)-NCRFLQG are separated from PpSB1-LOV- and PpSB2-LOV-like sequences comprising a noncanonical Y(Q/R)DCRFLQG motif. While the latter class is restricted to γ-proteobacterial lineages, proteins of the first class are dispersed throughout α-, β-, and γ-proteobacteria. This observation suggests a niche specific conservation of "short" LOV protein architectures and thus hints at distinct blue light responses in those bacterial lineages. Moreover, the evolutionary conservation of fast- and slow-reverting LOV photoreceptors in *P. putida* (strains KT2440 and W619) suggests the functional importance of evolutionarily conserved recovery-kinetic properties. We previously identified residues R61 and R66 as the key determinants for the slow dark recovery of PpSB1-LOV.[7,25] In the X-ray structure of PpSB1-LOV, R61 and R66 together with two conserved arginines in all LOV proteins (R54 and R70, PpSB1-LOV numbering) form an unusual cluster of charged residues coordinating the FMN phosphate.[7] Interchange of those two residues with their counterparts in the fast-reverting PpSB2-LOV protein (H61 and I66) resulted in an acceleration of the dark recovery by a factor of ∼280.[7] This dark recovery-determining structural feature is likely conserved in the two *P. putida* W619 LOV proteins, as the respective positions are occupied by either two arginines in the slow-reverting W619_1-LOV protein or a histidine and a leucine residue in the fast-reverting W619_2-LOV protein (highlighted

dx.doi.org/10.1021/bi400311r | *Biochemistry* 2013, 52, 4460−4473

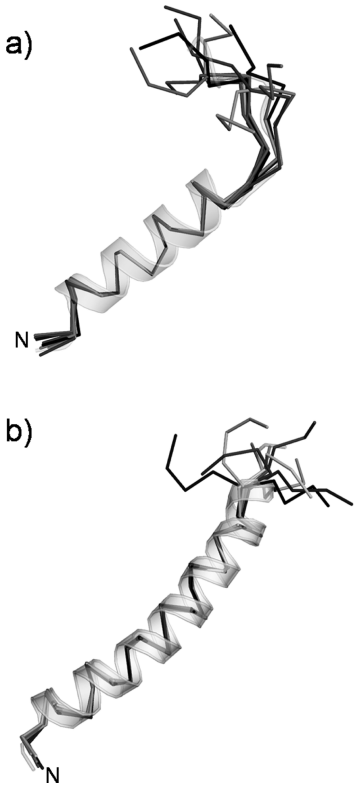

Figure 6. Ensemble of the 10 NMR-derived structures of PpSB1-Jα (a) and PpSB2-Jα (b) selected on the basis of energy from an ensemble of 250 structures. The polypeptide backbone of the 10 lowest-energy structures is shown as a ribbon (gray to black). The energy-minimized average structure is superimposed on the ensemble (colored white, transparent cartoon representation).

in red in Figure 1a of the Supporting Information). The other very slow-reverting LOV proteins (SBW25-LOV and Pf0-1-LOV) invariably contain an arginine at the position corresponding to R61 of PpSB1-LOV. Interestingly, in the two very-slow-reverting *P. fluorescens* LOV proteins, the position corresponding to R66 in PpSB1-LOV is occupied by a nonpolar leucine residue (see Figure 1a of the Supporting Information). Thus, additional structural features seem to contribute to the very slow dark recovery of the two *P. fluorescens* LOV proteins.

While the physiological role of both *P. putida* KT2240 LOV proteins remains elusive, experimental evidence of a functional role of a bacterial "short" LOV protein was recently provided for the "short" LOV protein RsLOV of *R. sphaeroides* 2.4.1.[24] Although small physiological similarities exist between the anoxygenic phototroph *R. sphaeroides* and the saprotrophic chemotroph *P. putida*, the study nevertheless proves that bacterial LOV proteins lacking fused effector domains can act as genuine blue light sensors, probably transducing the signal via protein−protein interactions with as yet unidentified downstream regulators. As a mode of signal transduction, changed surface properties caused by blue light-induced conformational changes in the LOV protein would provide a feasible mechanism for altering protein−protein interactions. A similar mechanism has been suggested for the fungal "short" LOV protein VVD of *Neurospora*.[57]

Conserved C-Terminal Jα-Helices Play an Essential Role in the Folding and Solubility of Pseudomonadaceae "Short" LOV Proteins. The CD spectroscopic data for the five Pseudomonadaceae "short" LOV proteins presented here as well as CD and NMR data for the two Jα-helix peptides suggest an evolutionary conservation and thus conserved structural role of the two N- and C-terminal auxiliary structural elements. For both PpSB1-LOV and PpSB2-LOV, the two elements need to be present to yield a soluble functional protein in *E. coli*. Hereby, the C-terminal Jα-helix seems to be more important, because its removal resulted in a nearly complete loss of solubility. This is in contrast to multidomain LOV photoreceptors, where both structural elements can be readily removed without the loss of protein solubility.[58−60] Hence, they appear to be integral for the functionality of the LOV sensory system. Thus, it is tempting to speculate that in the case of the Pseudomonadaceae "short" LOV proteins, the protruding C-terminal Jα-helices represent candidate structural elements whose coiled-coil-like interaction in the dimeric protein might be altered to modulate surface properties and thus could promote or impede protein−protein interactions in a given conformational state (light or dark).

CD and NMR Spectroscopic Studies Reveal Robust Folding of the Isolated Jα-Helix Peptides and Suggest a Certain Degree of Quaternary Structural Flexibility That Might Allow Signal Transduction. CD spectra as well as the solution NMR data presented here indicate α-helical secondary structure for the isolated PpSB1-Jα and PpSB2-Jα peptides at 1 °C in aqueous solution or at 25 °C in the presence of minimal amounts of the helix-stabilizing agent TFE. Both peptide CD spectra recorded at 1 °C in aqueous solution show minima at 222 and 208 nm as well as a maximum at ∼190 nm. These are signature features of helical secondary structure representing the n → π^* transition (∼222 nm) and $\pi \rightarrow \pi^*$ exciton split transition (∼190 and ∼208 nm) of peptide bonds.[61] The ellipticity ratio $[\Theta_{222}]/[\Theta_{208}]$ has previously been used as an indicator of coiled-coil formation of peptides.[62,63] Hereby, noncoiled helices show a ratio of ∼0.8, whereas coiled-coil structures yield values close to 1.[62] Mechanistically, this is due to the fact that in coiled coils the parallel polarized amide $\pi \rightarrow \pi^*$ transition becomes less dichroic, which effectively reduces the negativity of $[\Theta_{208}]$. Because $[\Theta_{222}]$ is not affected, the $[\Theta_{222}]/[\Theta_{208}]$ ratio increases to ∼1. For PpSB1-Jα and PpSB2-Jα, $[\Theta_{222}]/[\Theta_{208}]$ ratios are ∼0.67 and ∼0.89, respectively. Thus, coiled-coil formation is not apparent from CD spectra recorded for the two isolated Jα-helix peptides studied in aqueous solution, even at low temperatures.

The superimposition of the NMR-derived peptide structure of PpSB1-Jα with the respective structural element in the full-length crystal structure (PDB entry 3SW1) yields backbone and all-atom rmsd values of 0.362 and 0.919 Å, respectively. Thus, while the general folding is conserved in both crystal and solution, the Jα-helix structural elements apparently possess a certain degree of quaternary structural flexibility. They exist as an isolated helix in solution or packed as a tight coiled coil in the context of the full-length protein in the crystal. Please note that we cannot rule out completely that Jα-helix coiled-coil formation as observed in the PpSB1-LOV crystal structure is an artifact related to crystal packing. While the data for truncated PpSB1-LOV and PpSB2-LOV protein constructs presented here as well as size-exclusion chromatographic data[25] argue against this scenario, the issue could be resolved unequivocally only by obtaining high-resolution NMR structures of the PpSB1-LOV protein. More likely, the conformational flexibility observed for the Jα-helix element in solution and the crystal structure is related to coiled-coil instability imposed by the

short sequence length of the PpSB1-LOV and PpSB2-LOV Jα-helices. Thus, it appears that the Jα-helix coiled coil observed in the crystal is not sufficiently stable to promote coiled-coil formation in solution. Anchoring of the Jα-helix at the C-terminus of the LOV core in the full-length protein might impose dynamic and distance restraints on the orientation of the Jα-helices and thus might promote coiled-coil formation as observed in the crystal structure. Please note that direct interactions between the PpSB1-LOV core subunits are absent in the dimeric crystal structure. In the full-length protein, subunit association is solely stabilized by contacts mediated by the C-terminal Jα-helix and the N-terminal cap (A′α-helix).[7] Thus, both structural elements seem to be crucial for dimer formation of the full-length protein, and hence, Jα-helix coiled-coil formation as seen in the crystal structure might be possible only in the presence of the dimer contact-mediating N-cap.

C-Terminal Jα-Helices as the Potential "Missing" Effector Domain of the Pseudomonadaceae "Short" LOV Protein Family: Implications for the Design of LOV-Based Optogenetic Tools. Given the structural features discussed above, the protruding C-terminal Jα-helices could well represent the missing effector domain of the Pseudomonadaceae "short" LOV protein family whose interaction with, as yet unidentified, downstream signaling partners could be modulated by blue light. Recently, a dimer arrangement similar to that seen in the PpSB1-LOV crystal structure has been suggested for the *B. subtilis* YtvA photoreceptor,[9,64] PAS domains of histidine kinase chemosensory two-component systems (TCS),[21,65−67] and has been implied for artificially constructed LOV-based optogenetic switches.[19,21] The data presented here as well as recently published X-ray crystallographic evidence[7] highlight the possibility of using "short" LOV proteins as sensory switches for the construction of LOV-based optogenetic tools. Hereby, they could be used either in *cis*, by fusion of an artificial effector domain module,[19−21] or in *trans*, employing an as yet unidentified regulatory protein[68] or even by using *de novo* designed binding proteins as regulatory modules.[69]

CONCLUSIONS

Our study provides a solely sequence-based criterion for differentiation of PpSB1-LOV- and PpSB2-LOV-like sequences from the vast variety of other ("short") LOV proteins found in databases.[70] At the same time, we provide evidence of the conservation of recovery kinetic properties supporting a classification into slow- and fast-reverting Pseudomonadaceae "short" LOV proteins and show that N- and C-terminal helical structural elements are conserved features of this class of LOV photoreceptors. Given the structural similarity of PAS-based chemosensory TCS as well as the proposed structure of recently developed LOV-based optogenetic tools used for the control of gene expression,[19−21] the adaptability of Pseudomonadaceae "short" LOV proteins as sensory modules for the design of LOV-based optogenetic switches can be anticipated. Moreover, given their diverse photochemical properties with respect to fast and slow dark recovery reactions, their different signaling state stabilities could be utilized to construct switches with tunable sensitivities and response times.[71]

ASSOCIATED CONTENT

Supporting Information

Oligonucleotides used in this study, sequence information for all bacterial "short" LOV protein sequences depicted in Figure 1, HPLC−SEC and HPLC chromophore acceptance analyses, amino acid sequence alignment of bacterial "short" LOV proteins, CD spectroscopic analysis of PpSB1-Jα and PpSB2-Jα thermal unfolding, and NOE pattern and residue-wise secondary structure propensity scores (SSP) for PpSB1-Jα and PpSB2-Jα. This material is available free of charge via the Internet at http://pubs.acs.org.

Accession Codes

NMR chemical shift information for PpSB1-Jα and PpSB2-Jα has been deposited in the Biological Magnetic Resonance Databank as entries 18159 and 18160 and the Protein Databank Europe as entries 2YON and 2YOM, respectively.

AUTHOR INFORMATION

Corresponding Author

*E-mail: u.krauss@fz-juelich.de. Phone: ++49 2461 61 2939. Fax: ++49 2461 61 2490.

Author Contributions

R.R. and K.J. contributed equally to this work.

Funding

This work was supported by the NRW Research School BioStruct and the "Fit for Excellence"-Fonds of the Heinrich-Heine-Universität Düsseldorf.

Notes

The authors declare no competing financial interest.

ACKNOWLEDGMENTS

We thank Dr. Wojtek Augustyniak (Conformetrix Ltd., Manchester, U.K.) for his initial help with peptide NMR assignments and Dr. Melanie Schwarten (Institut de Biologie Structurale Jean Pierre Ebel, Grenoble, France) for her help with peptide NMR assignments and valuable support and suggestions during the initial phase of the project. K.-E.J. and U.K. acknowledge the excellent technical support provided by Esther Knieps-Grünhagen, Maja Piqueray, and Astrid Wirtz.

ABBREVIATIONS

LOV, light, oxygen, voltage; FMN, flavin mononucleotide; phot, phototropin; rmsd, root-mean-square deviation; CD, circular dichroism.

REFERENCES

(1) Herrou, J., and Crosson, S. (2011) Function, structure and mechanism of bacterial photosensory LOV proteins. *Nat. Rev. Microbiol. 9*, 713−723.

(2) Krauss, U., Minh, B. Q., Losi, A., Gärtner, W., Eggert, T., von Haeseler, A., and Jaeger, K. E. (2009) Distribution and phylogeny of light-oxygen-voltage-blue-light-signaling proteins in the three kingdoms of life. *J. Bacteriol. 191*, 7234−7242.

(3) Möglich, A., Ayers, R. A., and Moffat, K. (2009) Structure and signaling mechanism of Per-ARNT-Sim domains. *Structure 17*, 1282−1294.

(4) Zoltowski, B. D., and Gardner, K. H. (2011) Tripping the light fantastic: Blue-light photoreceptors as examples of environmentally modulated protein-protein interactions. *Biochemistry 50*, 4−16.

(5) Losi, A., and Gärtner, W. (2008) Bacterial bilin- and flavin-binding photoreceptors. *Photochem. Photobiol. Sci. 7*, 1168−1178.

(6) Möglich, A., Yang, X., Ayers, R. A., and Moffat, K. (2010) Structure and function of plant photoreceptors. *Annu. Rev. Plant Biol. 61*, 21−47.

(7) Circolone, F., Granzin, J., Jentzsch, K., Drepper, T., Jaeger, K. E., Willbold, D., Krauss, U., and Batra-Safferling, R. (2012) Structural

basis for the slow dark recovery of a full-length LOV protein from *Pseudomonas putida*. *J. Mol. Biol. 417*, 362−374.
(8) Halavaty, A. S., and Moffat, K. (2007) N- and C-terminal flanking regions modulate light-induced signal transduction in the LOV2 domain of the blue light sensor phototropin 1 from *Avena sativa*. *Biochemistry 46*, 14001−14009.
(9) Möglich, A., and Moffat, K. (2007) Structural basis for light-dependent signaling in the dimeric LOV domain of the photosensor YtvA. *J. Mol. Biol. 373*, 112−126.
(10) Nash, A. I., McNulty, R., Shillito, M. E., Swartz, T. E., Bogomolni, R. A., Luecke, H., and Gardner, K. H. (2011) Structural basis of photosensitivity in a bacterial light-oxygen-voltage/helix-turn-helix (LOV-HTH) DNA-binding protein. *Proc. Natl. Acad. Sci. U.S.A. 108*, 9449−9454.
(11) Vaidya, A. T., Chen, C. H., Dunlap, J. C., Loros, J. J., and Crane, B. R. (2011) Structure of a light-activated LOV protein dimer that regulates transcription. *Sci. Signaling 4*, ra50.
(12) Crosson, S., and Moffat, K. (2001) Structure of a flavin-binding plant photoreceptor domain: Insights into light-mediated signal transduction. *Proc. Natl. Acad. Sci. U.S.A. 98*, 2995−3000.
(13) Crosson, S., and Moffat, K. (2002) Photoexcited structure of a plant photoreceptor domain reveals a light-driven molecular switch. *Plant Cell 14*, 1067−1075.
(14) Fedorov, R., Schlichting, I., Hartmann, E., Domratcheva, T., Fuhrmann, M., and Hegemann, P. (2003) Crystal structures and molecular mechanism of a light-induced signaling switch: The Phot-LOV1 domain from *Chlamydomonas reinhardtii*. *Biophys. J. 84*, 2474−2482.
(15) Drepper, T., Krauss, U., Meyer zu Berstenhorst, S., Pietruszka, J., and Jaeger, K. E. (2011) Lights on and action! Controlling microbial gene expression by light. *Appl. Microbiol. Biotechnol. 90*, 23−40.
(16) Krauss, U., Drepper, T., and Jaeger, K. E. (2011) Enlightened enzymes: Strategies to create novel photoresponsive proteins. *Chemistry 17*, 2552−2560.
(17) Krauss, U., Lee, J., Benkovic, S. J., and Jaeger, K. E. (2010) LOVely enzymes: Towards engineering light-controllable biocatalysts. *Microb. Biotechnol. 3*, 15−23.
(18) Möglich, A., and Moffat, K. (2010) Engineered photoreceptors as novel optogenetic tools. *Photochem. Photobiol. Sci. 9*, 1286−1300.
(19) Möglich, A., Ayers, R. A., and Moffat, K. (2009) Design and signaling mechanism of light-regulated histidine kinases. *J. Mol. Biol. 385*, 1433−1444.
(20) Ohlendorf, R., Vidavski, R. R., Eldar, A., Moffat, K., and Möglich, A. (2012) From dusk till dawn: One-plasmid systems for light-regulated gene expression. *J. Mol. Biol. 416*, 534−542.
(21) Möglich, A., Ayers, R. A., and Moffat, K. (2010) Addition at the molecular level: Signal integration in designed Per-ARNT-Sim receptor proteins. *J. Mol. Biol. 400*, 477−486.
(22) Zoltowski, B. D., Schwerdtfeger, C., Widom, J., Loros, J. J., Bilwes, A. M., Dunlap, J. C., and Crane, B. R. (2007) Conformational switching in the fungal light sensor Vivid. *Science 316*, 1054−1057.
(23) Hendrischk, A. K., Moldt, J., Frühwirth, S. W., and Klug, G. (2009) Characterization of an unusual LOV domain protein in the α-proteobacterium *Rhodobacter sphaeroides*. *Photochem. Photobiol. 85*, 1254−1259.
(24) Metz, S., Jäger, A., and Klug, G. (2012) Role of a short light, oxygen, voltage (LOV) domain protein in blue light- and singlet oxygen-dependent gene regulation in *Rhodobacter sphaeroides*. *Microbiology 158*, 368−379.
(25) Jentzsch, K., Wirtz, A., Circolone, F., Drepper, T., Losi, A., Gärtner, W., Jaeger, K. E., and Krauss, U. (2009) Mutual exchange of kinetic properties by extended mutagenesis in two short LOV domain proteins from *Pseudomonas putida*. *Biochemistry 48*, 10321−10333.
(26) Krauss, U., Losi, A., Gärtner, W., Jaeger, K.-E., and Eggert, T. (2005) Initial characterization of a blue-light sensing, phototropin-related protein from *Pseudomonas putida*: A paradigm for an extended LOV construct. *Phys. Chem. Chem. Phys. 7*, 2804−2811.
(27) Studier, F. W. (2005) Protein production by auto-induction in high-density shaking cultures. *Protein Expression Purif. 41*, 207−234.
(28) Jentzsch, K., Wirtz, A., Circolone, F., Drepper, T., Losi, A., Gärtner, W., Jaeger, K. E., and Krauss, U. (2009) Mutual exchange of kinetic properties by extended mutagenesis in two short LOV domain proteins from *Pseudomonas putida*. *Biochemistry 48*, 10321−10333.
(29) Sambrook, J., Russel, D. W. (2001), Molecular cloning: a laboratory manual. Cold Spring Harbor Laboratory Press, Plainview, NY.
(30) Laemmli, U. (1970) Cleavage of structural proteins during the assembly of the head of bacteriophage T4. *Nature 227*, 680−685.
(31) Bradford, M. M. (1976) A rapid and sensitive method for the quantitation of microgram quantities of protein utilizing the principle of protein-dye binding. *Anal. Biochem. 72*, 248−254.
(32) Buttani, V., Losi, A., Eggert, T., Krauss, U., Jaeger, K.-E., Cao, Z., and Gärtner, W. (2007) Conformational analysis of the blue-light sensing protein YtvA reveals a competitive interface for LOV-LOV dimerization and interdomain interactions. *Photochem. Photobiol. Sci. 6*, 41−49.
(33) Delaglio, F., Grzesiek, S., Vuister, G. W., Zhu, G., Pfeifer, J., and Bax, A. (1995) NMRPipe: A multidimensional spectral processing system based on UNIX pipes. *J. Biomol. NMR 6*, 277−293.
(34) Vranken, W. F., Boucher, W., Stevens, T. J., Fogh, R. H., Pajon, A., Llinas, M., Ulrich, E. L., Markley, J. L., Ionides, J., and Laue, E. D. (2005) The CCPN data model for NMR spectroscopy: Development of a software pipeline. *Proteins 59*, 687−696.
(35) Brunger, A. T. (2007) Version 1.2 of the Crystallography and NMR system. *Nat. Protoc. 2*, 2728−2733.
(36) Linge, J. P., and Nilges, M. (1999) Influence of non-bonded parameters on the quality of NMR structures: A new force field for NMR structure calculation. *J. Biomol. NMR 13*, 51−59.
(37) Koradi, R., Billeter, M., and Wüthrich, K. (1996) MOLMOL: A program for display and analysis of macromolecular structures. *J. Mol. Graphics 14*, 29−32 , 51−55.
(38) *PyMol* (2010) Schrödinger, LLC.
(39) Vriend, G. (1990) WHAT IF: A molecular modeling and drug design program. *J. Mol. Graphics 8*, 29 , 52−56.
(40) Davis, I. W., Leaver-Fay, A., Chen, V. B., Block, J. N., Kapral, G. J., Wang, X., Murray, L. W., Arendall, W. B., III, Snoeyink, J., Richardson, J. S., and Richardson, D. C. (2007) MolProbity: All-atom contacts and structure validation for proteins and nucleic acids. *Nucleic Acids Res. 35*, W375−W383.
(41) Marsh, J. A., Singh, V. K., Jia, Z., and Forman-Kay, J. D. (2006) Sensitivity of secondary structure propensities to sequence differences between α- and γ-synuclein: Implications for fibrillation. *Protein Sci. 15*, 2795−2804.
(42) Krieger, E., Koraimann, G., and Vriend, G. (2002) Increasing the precision of comparative models with YASARA NOVA: A self-parameterizing force field. *Proteins 47*, 393−402.
(43) Altschul, S. F., and Koonin, E. V. (1998) Iterated profile searches with PSI-BLAST: A tool for discovery in protein databases. *Trends Biochem. Sci. 23*, 444−447.
(44) Schultz, J., Milpetz, F., Bork, P., and Ponting, C. P. (1998) SMART, a simple modular architecture research tool: Identification of signaling domains. *Proc. Natl. Acad. Sci. U.S.A. 95*, 5857−5864.
(45) Notredame, C., Higgins, D. G., and Heringa, J. (2000) T-COFFEE: A novel method for fast and accurate multiple sequence alignment. *J. Mol. Biol. 302*, 205−217.
(46) Nicholas, K., Nicholas, H. J., and Deerfield, D. (1997) GeneDoc: Analysis and Visualization of Genetic Variation. *EMBNEWS 4*, 14.
(47) Stamatakis, A., Ludwig, T., and Meier, H. (2005) RAxML-III: A fast program for maximum likelihood-based inference of large phylogenetic trees. *Bioinformatics 21*, 456−463.
(48) Gruber, M., Soding, J., and Lupas, A. N. (2006) Comparative analysis of coiled-coil prediction methods. *J. Struct. Biol. 155*, 140−145.
(49) Kyte, J., and Doolittle, R. F. (1982) A simple method for displaying the hydropathic character of a protein. *J. Mol. Biol. 157*, 105−132.

(50) Perczel, A., Hollosi, M., Tusnady, G., and Fasman, G. D. (1991) Convex constraint analysis: A natural deconvolution of circular dichroism curves of proteins. *Protein Eng. 4*, 669−679.
(51) Buttani, V., Losi, A., Eggert, T., Krauss, U., Jaeger, K.-E., Cao, Z., and Gärtner, W. (2007) Conformational analysis of the blue-light sensing protein YtvA reveals a competitive interface for LOV-LOV dimerization and interdomain interactions. *Photochem. Photobiol. Sci. 6*, 41−49.
(52) Studier, F. W. (2005) Protein production by auto-induction in high-density shaking cultures. *Protein Expression Purif. 41*, 207−234.
(53) Robson Marsden, H., and Kros, A. (2010) Self-assembly of coiled coils in synthetic biology: Inspiration and progress. *Angew. Chem., Int. Ed. 49*, 2988−3005.
(54) Brahms, S., and Brahms, J. (1980) Determination of protein secondary structure in solution by vacuum ultraviolet circular dichroism. *J. Mol. Biol. 138*, 149−178.
(55) Greenfield, N. J. (2006) Using circular dichroism collected as a function of temperature to determine the thermodynamics of protein unfolding and binding interactions. *Nat. Protoc. 1*, 2527−2535.
(56) Sonnichsen, F. D., Van Eyk, J. E., Hodges, R. S., and Sykes, B. D. (1992) Effect of trifluoroethanol on protein secondary structure: An NMR and CD study using a synthetic actin peptide. *Biochemistry 31*, 8790−8798.
(57) Vaidya, A. T., Chen, C. H., Dunlap, J. C., Loros, J. J., and Crane, B. R. (2011) Structure of a light-activated LOV protein dimer that regulates transcription. *Sci. Signaling 4*, ra50.
(58) Buttani, V., Losi, A., Eggert, T., Krauss, U., Jaeger, K. E., Cao, Z., and Gärtner, W. (2007) Conformational analysis of the blue-light sensing protein YtvA reveals a competitive interface for LOV-LOV dimerization and interdomain interactions. *Photochem. Photobiol. Sci. 6*, 41−49.
(59) Fedorov, R., Schlichting, I., Hartmann, E., Domratcheva, T., Fuhrmann, M., and Hegemann, P. (2003) Crystal structures and molecular mechanism of a light-induced signaling switch: The Phot-LOV1 domain from *Chlamydomonas reinhardtii*. *Biophys. J. 84*, 2474−2482.
(60) Möglich, A., and Moffat, K. (2007) Structural Basis for Light-dependent Signaling in the Dimeric LOV Domain of the Photosensor YtvA. *J. Mol. Biol. 373*, 112−126.
(61) Han, S., and Hill, A. F. (2008) Analysis of PrP conformation using circular dichroism. *Methods Mol. Biol. 459*, 145−159.
(62) Dutta, K., Alexandrov, A., Huang, H., and Pascal, S. M. (2001) pH-induced folding of an apoptotic coiled coil. *Protein Sci. 10*, 2531−2540.
(63) Muhle-Goll, C., Gibson, T., Schuck, P., Schubert, D., Nalis, D., Nilges, M., and Pastore, A. (1994) The dimerization stability of the HLH-LZ transcription protein family is modulated by the leucine zippers: A CD and NMR study of TFEB and c-Myc. *Biochemistry 33*, 11296−11306.
(64) Ogata, H., Cao, Z., Losi, A., and Gärtner, W. (2009) Crystallization and preliminary X-ray analysis of the LOV domain of the blue-light receptor YtvA from *Bacillus amyloliquefaciens* FZB42. *Acta Crystallogr. F65*, 853−855.
(65) Cheung, J., Bingman, C. A., Reyngold, M., Hendrickson, W. A., and Waldburger, C. D. (2008) Crystal structure of a functional dimer of the PhoQ sensor domain. *J. Biol. Chem. 283*, 13762−13770.
(66) Reinelt, S., Hofmann, E., Gerharz, T., Bott, M., and Madden, D. R. (2003) The structure of the periplasmic ligand-binding domain of the sensor kinase CitA reveals the first extracellular PAS domain. *J. Biol. Chem. 278*, 39189−39196.
(67) Zhang, Z., and Hendrickson, W. A. (2010) Structural characterization of the predominant family of histidine kinase sensor domains. *J. Mol. Biol. 400*, 335−353.
(68) Yazawa, M., Sadaghiani, A. M., Hsueh, B., and Dolmetsch, R. E. (2009) Induction of protein-protein interactions in live cells using light. *Nat. Biotechnol. 27*, 941−945.
(69) Karanicolas, J., Corn, J. E., Chen, I., Joachimiak, L. A., Dym, O., Peck, S. H., Albeck, S., Unger, T., Hu, W., Liu, G., Delbecq, S., Montelione, G. T., Spiegel, C. P., Liu, D. R., and Baker, D. (2011) A de novo protein binding pair by computational design and directed evolution. *Mol. Cell 42*, 250−260.
(70) Pathak, G. P., Losi, A., and Gärtner, W. (2012) Metagenome-based screening reveals worldwide distribution of LOV-domain proteins. *Photochem. Photobiol. 88*, 107−118.
(71) Strickland, D., Lin, Y., Wagner, E., Hope, C. M., Zayner, J., Antoniou, C., Sosnick, T. R., Weiss, E. L., and Glotzer, M. (2012) TULIPs: Tunable, light-controlled interacting protein tags for cell biology. *Nat. Methods 9*, 379−384.